Research Paper

GEOSPHERE

GEOSPHERE; v. 14, no. 5

https://doi.org/10.1130/GES01637.1

9 figures; 3 tables

CORRESPONDENCE: william.cavazza@unibo.it

CITATION: Cavazza, W., Cattò, S., Zattin, M., Okay, A.I., and Reiners, P., 2018, Thermochronology of the Miocene Arabia-Eurasia collision zone of southeastern Turkey: Geosphere, v. 14, no. 5, https://doi.org/10.1130/GES01637.1.

Science Editor: Raymond M. Russo
Associate Editor: Michael L. Williams

Received 17 November 2017
Revision received 26 May 2018
Accepted 3 July 2018

Thermochronology of the Miocene Arabia-Eurasia collision zone of southeastern Turkey

William Cavazza[1], Silvia Cattò[1], Massimiliano Zattin[2], Aral I. Okay[3], and Peter Reiners[4]

[1]Department of Biological, Geological and Environmental Sciences, University of Bologna, 40126 Bologna, Italy
[2]Department of Geosciences, University of Padua, 35131 Padua, Italy
[3]Eurasia Institute of Earth Sciences, Istanbul Technical University, Maslak 34469, Istanbul, Turkey
[4]Department of Geosciences, University of Arizona, Tucson, Arizona 85721, USA

ABSTRACT

The Bitlis-Pütürge collision zone of SE Turkey is the area of maximum indentation along the >2400-km-long Assyrian-Zagros suture between Arabia and Eurasia. The integration of (*i*) fission-track analyses on apatites, (*ii*) (U-Th)/He analyses on zircons, (*iii*) field observations on stratigraphic and structural relationships, and (*iv*) preexisting U-Pb and Ar-Ar age determinations on zircons, amphiboles, and micas provides for the first time an overall picture of the thermochronometric evolution of this collisional orogen. The data set points to ubiquitous latest Cretaceous metamorphism of a passive margin sedimentary sequence and its igneous basement not only along the suture zone but across the entire width of the Anatolia-Tauride block north of the suture. During the early Paleogene the basement complex of the Bitlis and Pütürge massifs along the suture was rapidly exhumed due to extensional tectonics in a back-arc setting and eventually overlain by Eocene shallow-marine sediments. The entire Oligocene is characterized by a rather flat thermochronometric evolution in the Bitlis orogenic wedge, contrary to the widely held belief that this epoch marked the inception of the Arabia-Eurasia collision and was characterized by widespread deformation. Deposition of a thick Oligocene sedimentary succession in the Muş-Hınıs basin occurred in a retroarc foreland setting unrelated to continental collision. During the Middle Miocene, the Bitlis-Pütürge orogenic wedge underwent a significant and discrete phase of rapid growth by both frontal accretion, as shown by cooling/exhumation of the foreland deposits on both sides of the orogenic prism, and underplating, as shown by cooling/exhumation of the central metamorphic core of the orogenic wedge. We conclude that continental collision started in the mid-Miocene, as also shown by coeval thick syntectonic clastic wedges deposited in flexural basins along the Arabian plate northern margin and contractional reactivation of a number of preexisting structures in the European foreland.

INTRODUCTION

The >2400-km-long Bitlis-Zagros (Assyrian) suture zone in the Middle East (Fig. 1) marks the continental collision between Arabia and Eurasia. This is a major event in Earth's history, which isolated the Mediterranean and the Indian ocean, and has been linked to mid-Cenozoic global cooling, Red Sea rifting, extension in the Aegean region, inception of the North and East Anatolian strike-slip fault systems, and development of the Anatolian-Iranian continental plateau (e.g., Şengör and Kidd, 1979; Dewey et al., 1986; Jolivet and Faccenna, 2000; Barazangi et al., 2006; Robertson et al., 2007; Allen and Armstrong, 2008; Yılmaz et al., 2010). The age of the continental collision has been the topic of much debate, with proposed ages ranging widely from the Late Cretaceous to the Pliocene (Hall, 1976; Berberian and King, 1981; Şengör et al., 1985; Yılmaz, 1993; Alavi, 1994; Jolivet and Faccenna, 2000; Agard et al., 2005; Robertson et al., 2007; Allen and Armstrong, 2008; Okay et al., 2010; McQuarrie and van Hinsbergen, 2013). Exact determination of the timing of the continental collision is crucial not only for understanding the evolution of the Bitlis-Zagros collisional orogen but also for elucidating the chronology and causative mechanisms of more general syn- and post-collisional processes like (*i*) the development of large-scale strike-slip systems accommodating plate convergence and (*ii*) the development of continental plateaux. In the Bitlis-Pütürge massifs of southeastern Turkey, i.e., the area of maximum continental indentation, high-temperature radiometric systems indicate a discrete episode of high-pressure–low-temperature (*HP-LT*) metamorphism in the latest Cretaceous (Hempton, 1985; Okay et al., 1985; Oberhänsli et al., 2010, 2012, 2013; Rolland et al., 2012; Topuz et al., 2017) which has been interpreted as the result of the collision between Eurasia and either Arabia or a smaller microplate. The only low-temperature thermochronometric data set available for the same region (Okay et al., 2010) (based on fission-track analyses on apatite in samples from both the basement units and the sedimentary cover) points to a discrete phase of rapid mid-Miocene cooling/exhumation interpreted as the onset of the Arabia-Eurasia hard collision. The results by Okay et al. (2010) do not rule out the possibility that the documented episode of Miocene cooling was only the last stage of a longer thermochronometric evolution and that the collision could have started somewhat earlier. This paper advances the state of the knowledge on this crucial area by integrating new apatite fission-track (AFT) and ZrHe data (this study) with other radiometric data from the literature (U-Pb on zircon and Ar-Ar on amphiboles and micas). The data ultimately provides a more complete picture of the thermo-tectonic evolution of selected segments of the Arabia-Eurasia collision zone. The results of this study indicate that the basement complex of the Bitlis and Pütürge massifs along the Assyrian suture

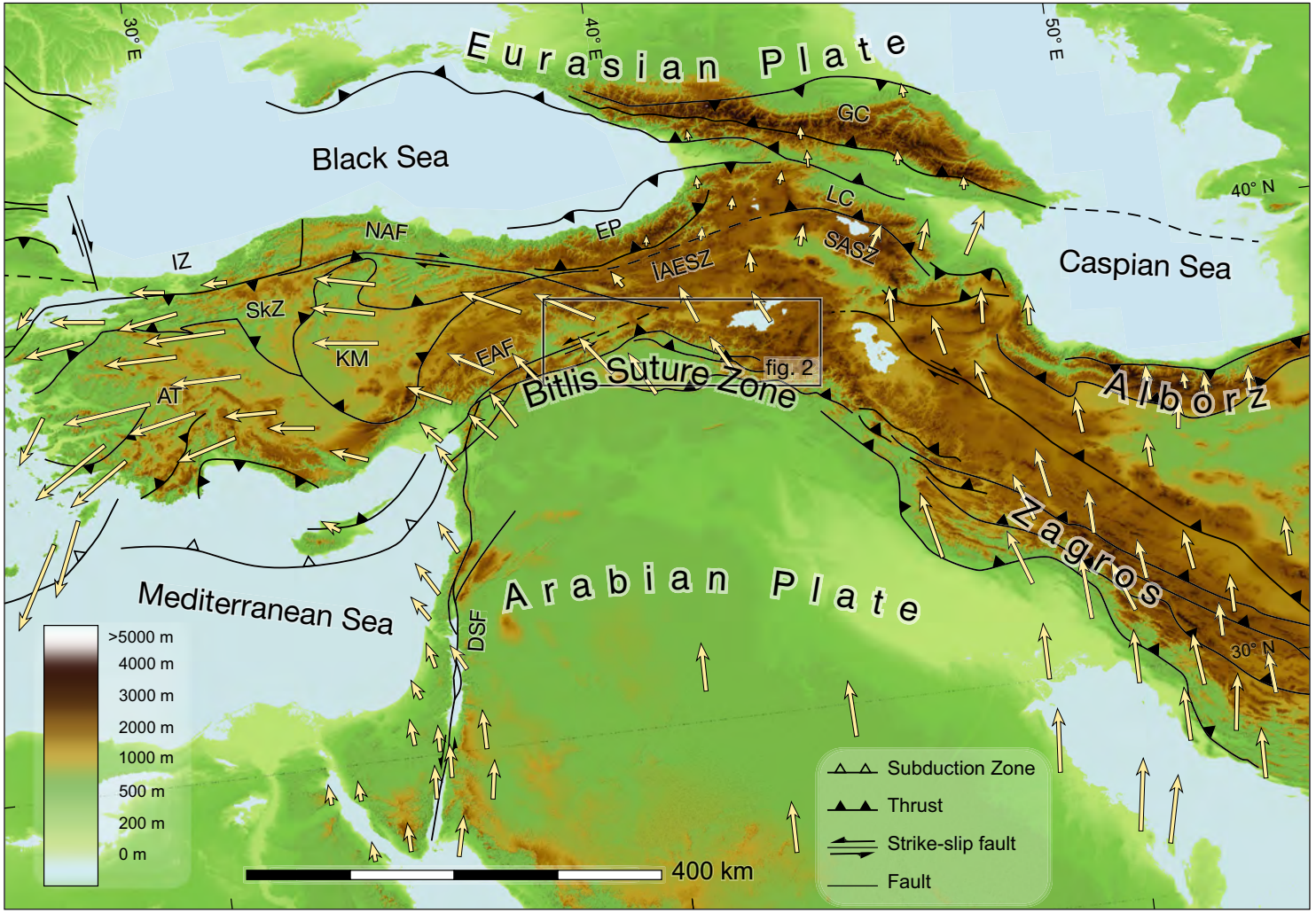

Figure 1. Overall tectonic sketch map of the Middle East. The box indicates the area shown in Figure 2. AT—Anatolide-Tauride terrane; IZ—Istanbul zone; SkZ—Sakarya zone; KM—Kirşehir Massif; NAF—North Anatolian fault; EAF—Eastern Anatolian fault; EP—Eastern Pontides; IAESZ—Izmir-Ankara-Erzincan suture zone; SASZ—Sevan-Akera suture zone; GC—Greater Caucasus; LC—Lesser Caucasus; DSF—Dead Sea fault. GPS vectors from Le Pichon and Kreemer (2010).

experienced the following thermochronometric evolution during the Cenozoic: (*i*) cooling/exhumation between ca. 65 and 55 Ma probably resulting from backarc extension; (*ii*) stable temperatures during the Oligocene except for the Muş-Hınıs retroarc foreland basin, where the sediments being deposited underwent progressive burial; and (*iii*) rapid cooling/exhumation during the Miocene, marking the collision between the Arabian and Eurasian plates.

GEOLOGICAL FRAMEWORK

The Bitlis-Pütürge Massif of southeastern Anatolia (Fig. 2) is a 500-km-long arcuate belt of allochthonous metamorphic rocks bordering the Arabian Platform to the south, from which it is separated by a narrow belt of Upper Cretaceous to Early Miocene mélange made of flysch and ophiolitic units (Hall,

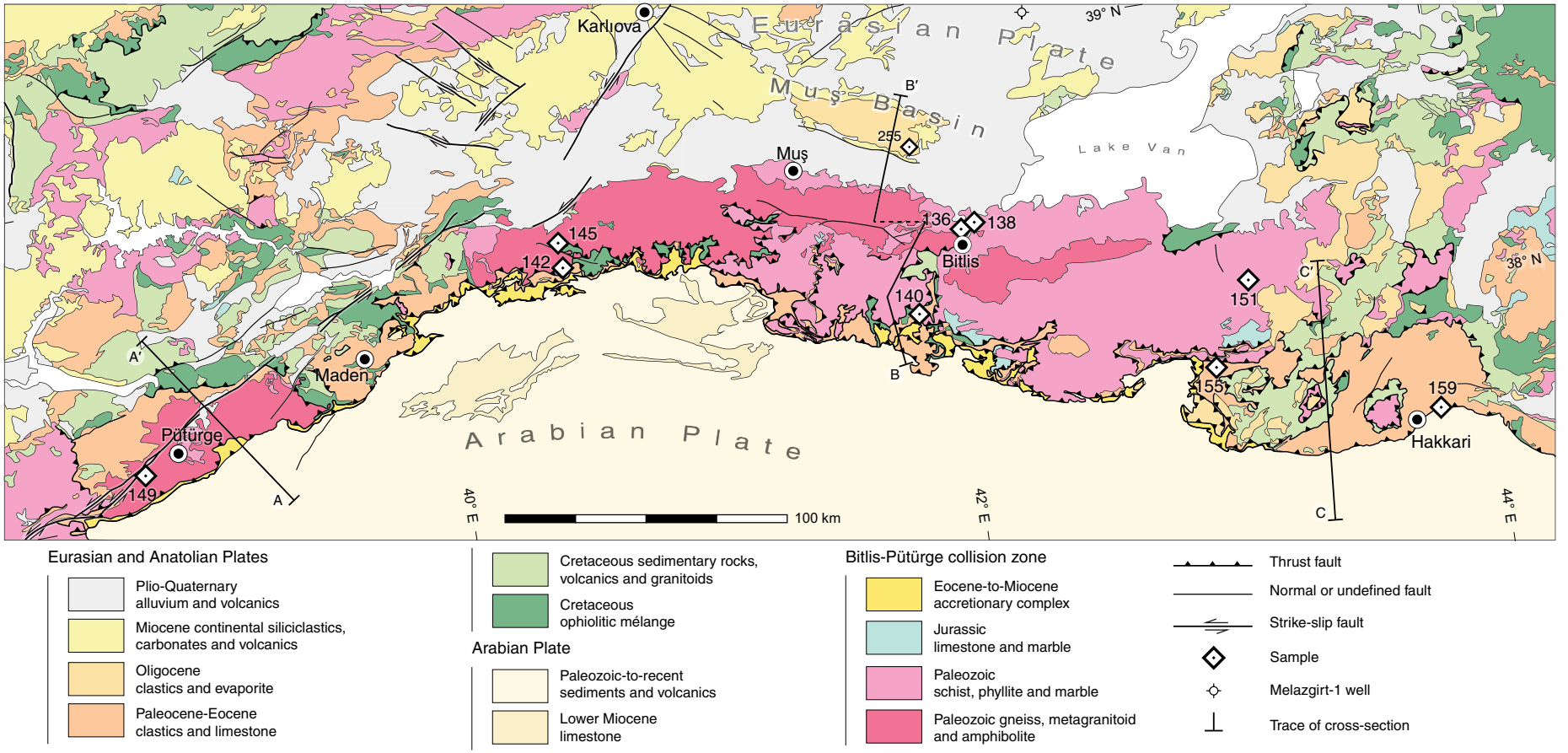

Figure 2. Geological sketch map of the Bitlis-Pütürge collision zone of southeastern Turkey (after Bilgic, 2002; Günay and Şenel, 2002; Şenel and Ercan, 2002; Tarhan, 2002).

1976; Perinçek, 1990; Yılmaz, 1993; Okay, 2008). The massif is made of a Precambrian basement and an overlying Phanerozoic sequence (Çağlayan et al., 1984; Göncüoğlu and Turhan, 1984; Okay et al., 1985). The Precambrian basement consists of polymetamorphosed gneiss, amphibolite, and mica schist. The overlying Phanerozoic sequence is mostly made of schist, phyllite, and marble and represents the Paleozoic-Mesozoic sedimentary cover of the Anatolide-Tauride terrane, which underwent low-to-medium grade metamorphism in the latest Cretaceous (83–69 Ma; Campanian-Maastrichtian) (Hempton, 1985; Oberhänsli et al., 2010, 2012, 2013; Karaoğlan et al., 2013; Rolland et al., 2012). In their regional synthesis, Şengör and Yılmaz (1981) proposed that Bitlis-Pütürge Massif deformation and metamorphism occurred in the Late Cretaceous in conjunction with ophiolite obduction from the north.

The present-day structural configuration of the Bitlis orogenic wedge is largely the result of south-verging post-Eocene thrusting, as shown by pervasive deformation of Middle-Late Eocene sedimentary units, commonly as broken formations and mélanges at the sole of the Bitlis-Pütürge metamorphic rocks (Yazgan et al., 1983; Perinçek, 1990; Bilgic, 2002; Günay and Şenel, 2002; Şenel and Ercan, 2002; Tarhan, 2002). Eocene thrusting was advocated by Hempton (1985), Yılmaz (1993), and Rolland et al. (2012). To the north, the imbricate structure of the Bitlis-Pütürge Massif is largely concealed by the Plio-Quaternary volcano-sedimentary rocks of the Anatolian Plateau, whereas to the south the massif overlies tectonically mélange complexes of various ages (e.g., Hakkäri Complex), as well as the thick sedimentary succession of the Arabian plate northern margin (e.g., Yılmaz, 1993).

The Bitlis-Pütürge Massif is generally considered to be the southern deformed margin of the Anatolide-Tauride terrane, originally separated from the Arabian Platform by the southern branch of the Neotethys (e.g., Barrier and Vrielynk, 2008; Stampfli and Hochard, 2009). It marks the area of maximum collisional indentation between Arabia and Eurasia, with widespread exposures of metamorphic rocks. In this region, the Assyrian suture is <150 km from the Late Cretaceous-Eocene Izmir-Ankara-Erzincan suture to the north (Fig. 1). These two suture zones mark the closure of the two branches of the western Neotethys (Barrier and Vrielynk, 2008; Stampfli and Hochard, 2009).

The area between the Izmir-Ankara-Erzincan and the Assyrian sutures is largely covered by the mostly Plio-Quaternary volcanic/volcaniclastic rocks of the Anatolian Plateau. Paleozoic sedimentary rocks metamorphosed in the Late Cretaceous (Santonian-Campanian; Topuz et al., 2017), crop out sparsely as inliers and are similar to those of the Bitlis-Pütürge Massif (both in terms of lithology and age of metamorphism). Metamorphism was interpreted to be synchronous with the emplacement of a very large body of ophiolite and underlying tectonic slices of ophiolitic mélange across the entire Anatolide-Tauride terrane (Şengör and Yılmaz, 1981; Okay and Tüysüz, 1999). Erosional remnants of this nappe of ophiolite and ophiolitic mélange occur in the study area. Cenozoic sedimentation over the narrow area between the Izmir-Ankara-Erzincan and the Assyrian sutures was influenced by flexural processes due to the load exerted on the lithosphere by the orogenic wedges associated with the two suture zones (e.g., Huvaz, 2009). In general terms, outcrop areas of Eocene sedimentary successions tend to be concentrated to the north, i.e., close to the Izmir-Ankara-Erzincan suture; whereas Oligocene–Early Miocene successions are concentrated to the south, close to the Bitlis suture (Bilgic, 2002; Günay and Şenel, 2002; Şenel and Ercan, 2002; Tarhan, 2002). A large outcrop area of latest Eocene-to-Early Miocene sedimentary rocks to the west of Lake Van (Fig. 2) is commonly referred to as Muş Basin (e.g., Akay et al., 1989; Sancay et al., 2006; Hüsing et al., 2009), but in reality is an inlier of a much larger sedimentary basin (Muş-Hınıs Basin) spanning virtually the entire area shown north of the Bitlis Massif in Figure 2 and for the most part concealed by the Plio-Quaternary volcano-sedimentary succession (Huvaz, 2009).

SAMPLES AND METHODS

Samples for apatite fission-track [AFT] and zircon (U-Th-Sm)/He [ZHe] analyses were collected along four transects across the Bitlis and Pütürge massifs and the collision zone, perpendicular to the strike of the main tectonic structures. Lithostratigraphic units from which the samples were taken comprise (*i*) the Bitlis and Pütürge metamorphic complexes, (*ii*) the Eocene sandstones of the Maden and Hakkari complexes, (*iii*) the Oligocene sandstones of the Muş-Hınıs foreland basin, and (*iv*) the Paleozoic sandstone units in the collision-induced faulted anticlines on the Arabian Plate (Fig. 2; Table 1). Samples analyzed for this paper are the same as those analyzed by Okay et al. (2010) except for an additional sample (TU-255) from the Muş-Hınıs Basin. New, multiple mineral separations were made in order to obtain enough apatite grains and a statistically robust number of fission-track measurements. This paper includes three new determinations of fission-track length distributions on apatite and seventeen new ZHe analyses on zircon. Integration of new analytical data with observations of stratigraphic/structural relationships and preexisting U-Pb and Ar-Ar age determinations on zircon, amphibole, and mica resulted in the definition of the thermochronological evolution of four samples.

Sample preparation and AFT analyses were carried out at the Department of Biological, Geological and Environmental Sciences of the University of

TABLE 1. APATITE FISSION-TRACK ANALYTICAL DATA

Sample	Coordinates (UTM)		Elevation (m)	Rock type	No. of crystals	Spontaneous		Induced		$P(\chi)^2$	Dosimeter		Age (Ma) ± 1σ	Mean confined track length (μm) ± SE	Std. dev.	No. of tracks measured
						ρ_s	N_s	ρ_i	N_i		ρ_d	N_d				
TU136	38S0251160	4260508	1642	Metasandstone	20	0.72	40	0.89	496	100.0	0.90	4293	13.4 ± 2.2	14.4 ± 0.2	1.24	51
TU138	38S0241967	4249698	1285	Gneiss	16	0.46	22	0.55	264	100.0	0.90	4281	13.8 ± 3.1	–	–	–
TU140	37S0753971	4234870	871	Sandstone	4	5.14	43	4.84	405	91.1	0.90	4256	17.5 ± 2.8	–	–	–
TU142	37S0634579	4267009	1208	Gneiss	–	–	–	–	–	–	–	–	–	–	–	–
TU145	37S0630748	4277901	1175	Metagranite	20	0.55	38	0.62	425	82.5	0.89	4219	14.6 ± 2.5	–	–	–
TU149	37S0476619	4240707	1395	Gneiss	20	1.60	112	1.44	1006	87.0	0.88	4181	18.0 ± 1.8	14.1 ± 0.2	1.35	72
TU151	38S0340100	4221763	2025	Chlorite schist	–	–	–	–	–	–	–	–	–	–	–	–
TU155	38S0321648	4195176	1607	Sandstone	20	0.88	53	1.18	711	65.1	1.01	4818	13.9 ± 2.1	15.2 ± 0.2	1.08	51
TU159	38S0396240	4162747	1342	Sandstone	6	0.53	14	0.39	102	75.4	1.00	4771	25.2 ± 7.2	–	–	–
TU255	37S0750864	4293994	1339	Sandstone	17	1.98	122	0.65	481	76.4	14.30	4679	53.3 ± 1.7	13.7 ± 0.2	1.38	62

Note: Central ages were calculated using dosimeter glass CN5 and ζ-CN5 = 367.45 ± 4.35 (analyst MZ). ρ_s—spontaneous track densities (×10^5 cm^{-2}) measured in internal mineral surfaces; Ns—total number of spontaneous tracks; ρ_i and ρ_d—induced and dosimeter track densities (×10^6 cm^{-2}) on external mica detectors (g = 0.5); N_i and N_d—total numbers of tracks; $P(\chi^2)$—probability of obtaining χ^2 value for degrees of freedom (where ν = number of crystals – 1); a probability >5% is indicative of a homogeneous population. Samples with a probability <5% were analyzed with the binomial peak-fitting method. SE—standard error; Std. Dev.—standard deviation.

Bologna, Italy. Apatite and zircon grains were concentrated by crushing and sieving, followed by hydrodynamic, magnetic, and heavy-liquid separation. Apatite grains were embedded in epoxy resin, polished in order to expose the internal surfaces within the grains, and spontaneous fission tracks (FT) were revealed by etching with 5N HNO_3 at 20 °C for 20 seconds. The mounts were then coupled with a low-uranium fission-track-free muscovite mica sheet (external detector method) and sent for irradiation with thermal neutrons (see Donelick et al., 2005, for details) at the Radiation Center of Oregon State University, USA. Nominal fluence of 9×10^{15} n cm^{-2} was monitored with a CN5 uranium-doped silicate glass dosimeter. Induced fission tracks were revealed by etching of the mica sheets in 40% HF for 45 minutes at 20 °C. Apatite grains from 24 samples were sent for irradiation, however, most samples had too low uranium to generate enough tracks for a reliable age determination. Eight samples yielded apatite suitable for fission-track analysis. Spontaneous and induced fission tracks were counted under an optical microscope at ×1250 magnification, using an automatic stage (FTStage system) plus a digitizing tablet. Central ages were calculated with the zeta calibration approach (Hurford and Green, 1983), using Durango (31.3 ± 0.3 Ma) and Fish Canyon Tuff (27.8 ± 0.2 Ma) age standards within grains exposing *c*-axis-parallel crystallographic planes.

Apatite track-length distributions were calculated by measuring horizontal confined tracks together with the angle between the track and the *c*-axis. Confined tracks constitute a small part of the FT population, therefore additional concentrates were mounted, polished, and etched for the analysis. Ultimately, four samples contained a statistically significant number of confined tracks. A quantitative evaluation of the thermal history of these four samples was carried out through modeling procedures, which find a range of cooling paths compatible with the apatite fission-track age and track-length distribution of each sample (Ketcham, 2005). In this work, inverse modeling of track-length data was performed using the HeFTy program (Ehlers et al., 2005), which generates the possible temperature-time (*T*-*t*) paths by a Monte Carlo algorithm. Predicted AFT data were calculated according to the Ketcham et al. (2007) annealing model for fission tracks revealed by etching. D_{par} values (i.e., the etch pit length) were used to define the annealing kinetic parameters of the grains and the original track length. All available geological constraints (intrusion ages, metamorphic events, depositional ages, and stratigraphic relationships) and the results of ZHe analyses were incorporated into the thermochronometric modeling of the four selected samples (see next section).

Seven samples taken from the Bitlis-Pütürge metamorphic complex and the Eocene sandstones of the Hakkäri complex were prepared for ZHe analyses. Handpicked zircon grains were photographed and measured for alpha-ejection correction following methods described in Reiners and Brandon (2006) and Hourigan et al. (2005). Helium analysis was performed at the Radiogenic Helium dating laboratory of the Department of Geosciences of the University of Arizona, USA. The packets containing the single crystals to be analyzed and the standard crystals were placed in a stainless steel planchet inside a laser cell and degassed under vacuum by heating with a Nd-YAG laser for 15 minutes at 1–5 W. Helium blanks (0.1–0.05 fmol ^{4}He) were determined by heating empty packets with the same procedure. The gas was then spiked with 4 pmol ^{3}He, condensed in a cryogenic trap at 16 K, then released at 37 K into a small volume with an activated getter and the source of a Balzer quadrupole mass spectrometer with Channeltron electron multiplier. Masses of HD and H^{3+} were measured to correct the ^{3}He/^{4}He measured ratios. The obtained ratios were referenced to ^{4}He standards measured in the same way. After ^{4}He measurement samples were retrieved from the laser cell, each packet was placed in a Teflon vial, spiked with calibrated ^{229}Th, ^{233}U, and ^{147}Sm solution and dissolved by high-temperature, multi-step dissolution using high-pressure vessels and concentrated HF-HNO_3, and HCl acid (Reiners, 2005). Isotope ratios were then measured at the University of Arizona on a high-resolution (single-collector) Element2 inductively coupled plasma–mass spectrometer.

ANALYTICAL RESULTS

Results of AFT analysis from the Bitlis-Pütürge collision zone and from the adjacent Muş-Hınıs Basin are reported in Table 1. AFT central ages from the orogenic wedge cluster tightly between 13.4 ± 2.2 and 18.0 ± 1.8 Ma. Sample TU-159 (an Eocene turbidite sandstone from the Hakkäri Complex) has a central age of 25.2 ± 7.2 Ma, significantly older than all other samples. Sample TU-255, an Oligocene turbidite sandstone from the Muş-Hınıs foreland basin, yielded an AFT central age of 53.3 ± 1.7 Ma, older than its depositional age. This implies that the sample was only partially reset because it never reached temperatures corresponding to the base of the partial annealing zone of apatite (~120 °C), as discussed below. Analyzed samples do not show any particular age-elevation correlation. All the samples passed the χ^2 test, indicating a single population of grains.

Table 2 provides a summary of (U-Th)/He analyses on zircon. All samples show a somewhat rapid cooling/exhumation through the partial retention zone. This is supported by (*i*) reproducible results of replicate analyses and (*ii*) no correlation of single grain ages with the equivalent sphere radius and eU (effective uranium). Therefore, the weighted mean of single grain ages adequately constrains the closure temperature of each sample. Most of the ZHe ages (samples TU-136, TU-142, TU-145, TU-149) cluster coherently between 44.2 and 37.0 Ma (Lutetian-Priabonian). The consistent results of replicate analyses of single samples indicate a rapid and widespread episode of cooling/exhumation in the Eocene. Sample TU-151 (Precambrian chlorite schist) yielded an age of 60.4 Ma, in line with higher temperature radiometric systems employed in the same area (Oberhänsli et al., 2010, 2012, 2013), and was unaffected by later heating. Sample TU-138 (Precambrian gneiss) yielded an Early Miocene weighted mean age (22.4 Ma). All ZHe results were incorporated into the thermochronometric modeling (see below).

The thermochronometric modeling of sample TU-149 (Precambrian gneiss; Pütürge Massif; Fig. 2) is well constrained by (*i*) a 77.5 ± 0.7 Ma Ar/Ar age on phengites from mica schists of the overlying Paleozoic metasedimentary sec-

TABLE 2. ZIRCON (U-Th)/He ANALYTICAL DATA

Sample	Raw age ± 2σ (Ma)	R_s (mm)	U (ppm)	Th (ppm)	^{4}He (nmol/g)	eU (ppm)	F_T ^{238}U	F_T ^{235}U	F_T ^{232}Th	Fully F_T corrected age ± σ (Ma)
TU136										
TU136_Zr2	29.1 ± 2.2	68	436	109	73	461.41	0.82	0.79	0.79	35.6 ± 1.3
TU136_Zr3	32.3 ± 2.4	43	482	47	86	493.00	0.72	0.68	0.68	44.7 ± 1.6
TU138										
TU138_Zr1	18.5 ± 0.4	48	125	100	15	148.07	0.75	0.71	0.71	25.0 ± 0.3
TU138_Zr2	14.6 ± 0.4	50	165	94	15	187.12	0.76	0.72	0.72	19.5 ± 0.3
TU138_Zr4	16.4 ± 1.2	44	180	129	19	210.18	0.73	0.69	0.69	22.7 ± 0.8
TU142										
TU142_Zr2	34.3 ± 1.0	46	290	166	61	329.27	0.74	0.70	0.70	46.7 ± 0.7
TU142_Zr3	31.0 ± 0.8	39	242	104	45	266.80	0.70	0.66	0.66	44.8 ± 0.6
TU142_Zr4	27.7 ± 0.8	37	848	1087	165	1103.95	0.68	0.64	0.64	41.1 ± 0.5
TU145										
TU145_Zr1	27.9 ± 0.8	48	2168	1339	374	2482.57	0.75	0.71	0.71	37.6 ± 0.5
TU145_Zr2	25.8 ± 0.6	47	2572	1405	404	2901.92	0.74	0.71	0.71	34.9 ± 0.4
TU145_Zr3	26.7 ± 0.8	39	1763	1101	292	2022.16	0.70	0.66	0.66	38.6 ± 0.5
TU149										
TU149_Zr1	22.7 ± 0.6	31	1266	153	160	1302.21	0.63	0.58	0.58	36.3 ± 0.5
TU149_Zr2	26.0 ± 0.8	35	958	162	140	995.75	0.67	0.62	0.62	39.0 ± 0.6
TU151										
TU151_Zr1	53.3 ± 1.4	58	188	63	58	202.21	0.790	0.759	0.759	67.7 ± 0.9
TU151_Zr2	37.9 ± 1.2	36	301	49	64	312.14	0.675	0.630	0.630	56.4 ± 0.8
TU151_Zr3	46.8 ± 1.4	68	572	109	151	597.02	0.820	0.794	0.794	57.2 ± 0.8
TU155										
TU155_Zr3	17.5 ± 0.4	36	327	263	37	389.14	0.672	0.628	0.628	26.3 ± 0.3

Note: F_T—retentivity of alpha particle in a sphere of varying radius; R_s—equivalent sphere radius.

tion nearby (Rolland et al., 2012), (*ii*) mid-Eocene sedimentary rocks nonconformably overlying the Pütürge basement complex (e.g., Bilgic, 2002) (Fig. 3), and by our own (*iii*) ZHe (Table 2) and (*iv*) AFT (Table 1) analyses. Following Late Cretaceous metamorphism, the sample underwent fairly rapid cooling and exhumation to near-surface conditions induced by extensional tectonics (Fig. 3B). This interpretation is supported by field stratigraphic relationships as the Precambrian gneisses in the area are nonconformably overlain by the Maden Complex, a thick volcano-sedimentary succession deposited in a short-lived (Middle-Late Eocene) backarc basin (Yiğitbaş and Yılmaz, 1996). Deposition of the Maden Complex induced progressive burial heating of basement sample TU-149 between ca. 45 and 39 Ma. Such burial heating is constrained by the ZHe analyses indicating that the sample cooled below 200 °C in the Late Eocene (Table 2; Fig. 3B). The Oligocene thermal evolution of the sample is rather flat until ca. 19 Ma (Burdigalian), when the best-fit curve derived from the study of the apatite fission-track length distribution (Fig. 3B) shows a sudden increase in the cooling rate.

Thermochronometric modeling of sample TU-136 (Paleozoic metasandstone; central Bitlis Massif; Fig. 2) is constrained by (*i*) two Late Cretaceous (Campanian; 84.4–73.8 Ma) (Oberhänsli et al., 2012, 2013) metamorphic ages from similar rock units along tectonic strike to the southeast (Table 3), (*ii*) Middle-Late Eocene sedimentary rocks nonconformably overlying the Bitlis basement complex (e.g., Tarhan, 2002) (Fig. 4), and by our own (*iii*) ZHe analyses (Table 2) and (*iv*) AFT analysis (Table 1). The track-length frequency distribution is platikurtic—the result of a long residence time in the partial annealing zone—with abundant long tracks (15–17 μm) indicating a later phase of rapid cooling (Fig. 4C). The thermochronometric evolution of this metasedimentary sample from the Bitlis Massif is similar to the one described above for the Precambrian gneisses of the Pütürge Massif. Again, after Late Cretaceous metamorphism, the sample was rapidly exhumed to the surface, as shown by the Middle-Late Eocene nonconformable sedimentary cover of the Kızılağaç Formation and its equivalents, including the Maden Complex of the western Bitlis-Pütürge Massif (Şengör et al., 2008). Results of ZHe analyses constrain further the statistical model and pre-

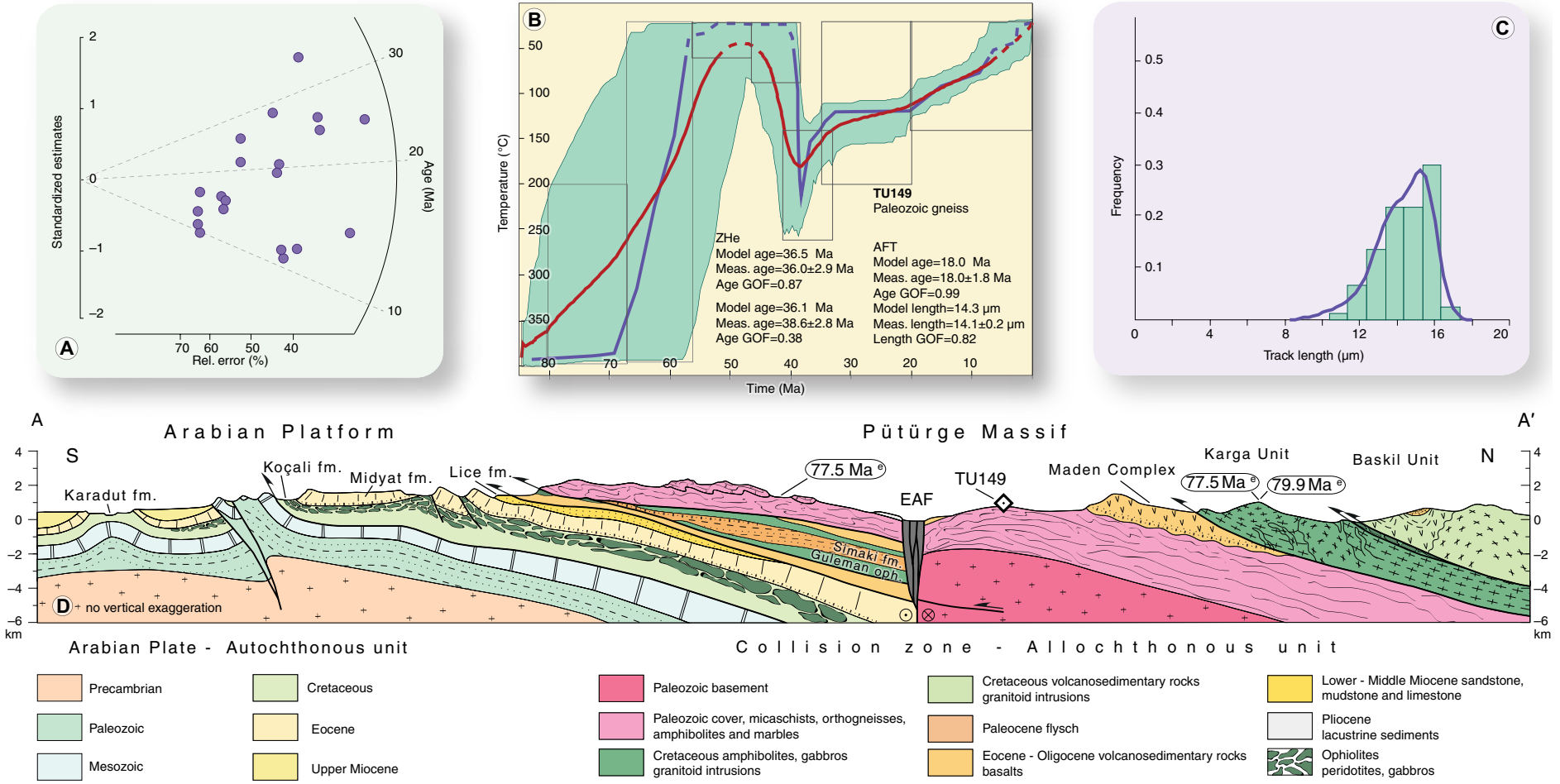

Figure 3. Summary of analytical results for sample TU-149 (Precambrian gneiss; Pütürge Massif) and geological cross-section A–A′ (see Fig. 2 for location). For details on radiometric ages reported in the figure, see Table 3. EAF—East Anatolian fault. (A) Radial plots of single-grain apatite fission-track (AFT) ages. (B) Time-temperature paths obtained from integrated inverse modeling of AFT data (this study), (U-Th)/He analyses on zircons (this study), Ar-Ar analysis on biotites, and U/Pb on zircons (Kiliç and Ateş, 2015). Green areas mark envelopes of statistically acceptable fit, and the thicker lines correspond to the most probable thermal histories: red line is the mean of all statistically acceptable paths; blue line is the best-fit *T-t* path. Parameters related to inverse modeling are reported: GOF, goodness-of-fit gives an indication about the fit between observed and predicted data (values closer to 1 are best). (C) Histogram showing the confined-track length distributions of apatite grains. (D) Geological cross-section of the Pütürge Massif (redrawn from Yazgan et al., 1983). No vertical exaggeration. See Figure 2 for location of trace of section.

scribe a phase of burial heating during the Middle Eocene (Fig. 4B). The entire duration of the Oligocene (and Early Miocene) is characterized by the residence of the sample at stable temperatures, corresponding to the base of the partial annealing zone of apatite (~120 °C). A sudden increase in the rate of cooling occurred at 15–12 Ma (Middle Miocene) depending on whether we consider the mean or best-fit curve (Fig. 4B).

An Early Oligocene sandstone sample (TU-255) from the lower portion of the Muş foreland basin fill (Yazledere Formation, Figs. 2 and 3) yielded a broad single-grain age distribution (Fig. 4E) and a bimodal track-length distribution (Fig. 4G), indicating a complex thermal history. AFT central age for this sample is 53.2 Ma (Table 1), i.e., older than its depositional age. This implies that the sample has not been completely reset, thus partially retaining the original

TABLE 3. COMPILATION OF PREEXISTING RADIOMETRIC DATA

Sample	Rock type	Coordinates (UTM)		Dated mineral	Method	Age (Ma)	±σ (Ma)
Bitlis Massif							
VAN 26[a]	metapelite	–		muscovite	$^{40}Ar/^{39}Ar$	69.8	0.4
VAN 27[a]	metapelite	–		muscovite	$^{40}Ar/^{39}Ar$	69.2	0.7
VAN 29[a]	metapelite	–		muscovite	$^{40}Ar/^{39}Ar$	68.8	2.2
VAN 36[a]	metapelite	–		muscovite	$^{40}Ar/^{39}Ar$	68.0	0.7
VAN 75[a]	metapelite	–		muscovite	$^{40}Ar/^{39}Ar$	73.8	7.7
VAN 75A[a]	metapelite	–		muscovite	$^{40}Ar/^{39}Ar$	73.8	7.7
VAN 76[a]	metapelite	–		muscovite	$^{40}Ar/^{39}Ar$	76.0	0.7
VAN 77[a]	metapelite	–		muscovite	$^{40}Ar/^{39}Ar$	78.8	0.6
VAN 75[b]	metapelite	–		phengite	$^{40}Ar/^{39}Ar$	73.8	7.7
VAN 75A[b]	metapelite	–		phengite	$^{40}Ar/^{39}Ar$	73.6	4.4
B157-1[g]	eclogite	–		zircon	U–Pb	82.4	0.9
B157-2[g]	eclogite	–		zircon	U–Pb	84.4	0.9
Pütürge Massif							
Loc28[c]	micaschist	37N 477060.9	4217244.7	phengite	$^{40}Ar/^{39}Ar$	77.5	0.7
Loc59[c]	amphibolites	37N 431046.1	4230447.3	amphibole	$^{40}Ar/^{39}Ar$	47.1	1.2
13TK51[d]	augen gneiss	–		zircon	U–Pb	551	6
13TK54[d]	augen gneiss	–		zircon	U–Pb	544	4
Sample[f]	micaschist	–		whole–rock	K–Ar	71.2	3.6
dk704[h]	metagranitic gneiss	–		zircon	U–Pb	84.2	1.1
dk173.8[h]	metapelitic schist	–		biotite	$^{40}Ar/^{39}Ar$	83.21	0.07
Baskil granitoids							
FK08-33[i]	granodiorite	N38°37′46.7″	E038°49′10.5″	apatite	fission track	48.39	8.92
FK08-36[i]	granodiorite	N38°38′11.1″	E038°49′46.1″	apatite	fission track	50.29	9.09
FK-06[i]	granite	N38°29′43.9″	E038°46′38.1″	apatite	fission track	40.17	5.14
FK08-38[i]	granodiorite			apatite	fission track	50.55	5.64
Maden Complex							
Loc46[c]	gabbro	37N 484693.9	4254696.6	amphibole	$^{40}Ar/^{39}Ar$	79.9	0.4
Loc46(duplicate)[c]	gabbro	37N 484693.9	4254696.7	amphibole	$^{40}Ar/^{39}Ar$	77.5	0.7
Keban-Malatya							
Loc49[c]	marble	37N 476355.5	4296643.1	muscovite	$^{40}Ar/^{39}Ar$	73.0	0.5
Ophiolite							
FK10[e]	rhyolite	–		zircon	U–Pb	74.6	4.4
FK48[e]	rhyolite	–		zircon	U–Pb	83.1	2.2

[a]Oberhänsli et al. (2012)
[b]Oberhänsli et al. (2010)
[c]Rolland et al. (2012)
[d]Beyarslan et al. (2016)
[e]Karaoğlan et al. (2013)
[f]Hempton (1985)
[g]Oberhänsli et al. (2013)
[h]Kiliç and Ateş (2015)
[i]Karaoğlan et al. (2016)

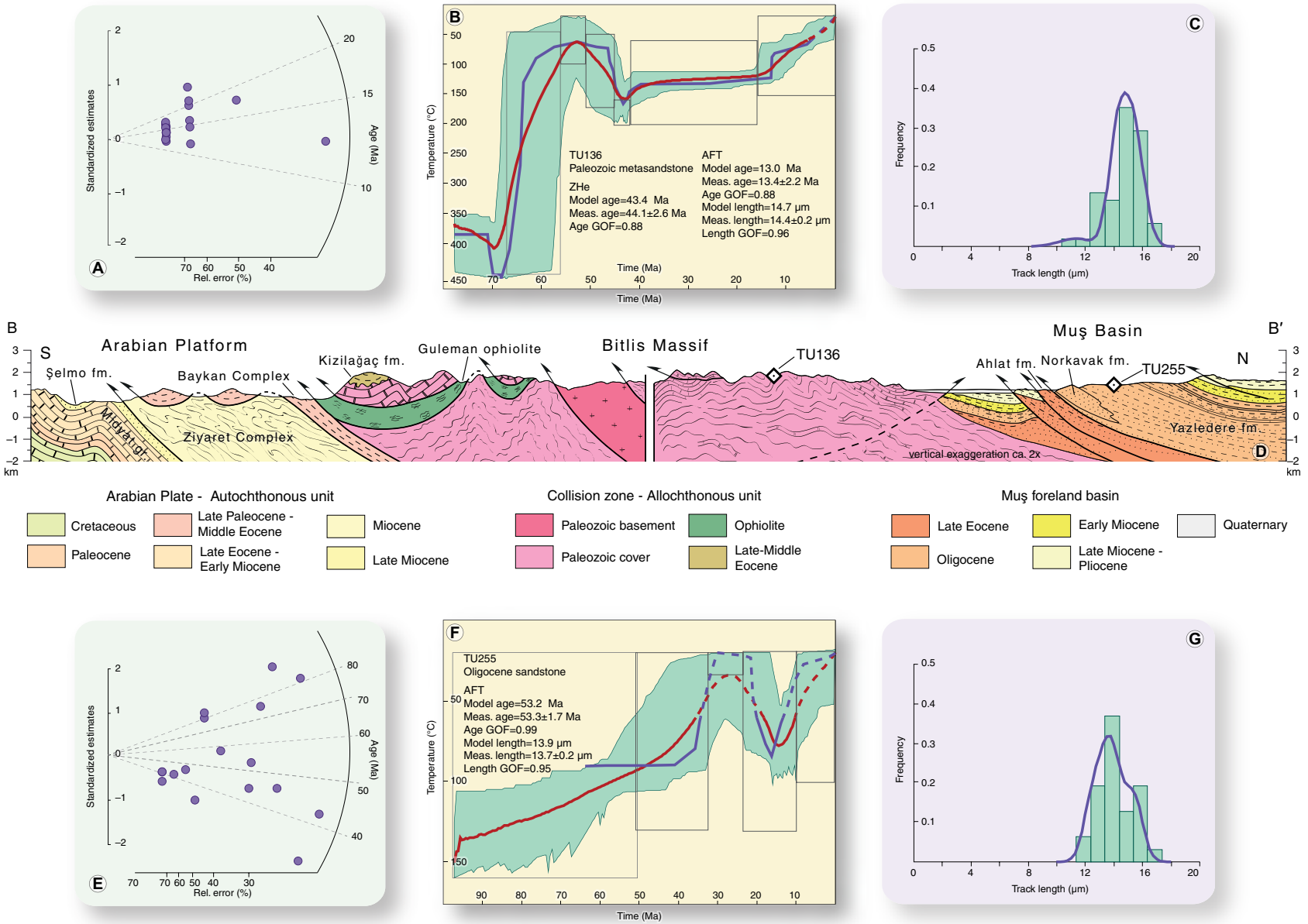

Figure 4. Summary of analytical results for samples TU-136 (Precambrian gneiss; Bitlis Massif) and TU-255 (Oligocene sandstone; Muş-Hınıs Basin). See Figure 2 for location. (A and E) Radial plots of single-grain apatite fission-track (AFT) ages. (B and F) Time-temperature paths obtained from integrated inverse modeling of AFT data (this study), (U-Th)/He analyses on zircons (this study), Ar-Ar analysis on biotites, and U/Pb on zircons (Kiliç and Ateş, 2015). Green areas mark envelopes of statistically acceptable fit, and the thicker lines correspond to the most probable thermal histories: red line is the mean of all statistically acceptable paths; blue line is the best-fit *T-t* path. Parameters related to inverse modeling are reported: GOF, goodness-of-fit gives an indication about the fit between observed and predicted data (values closer to 1 are best). (C and G) Histogram showing the confined-track length distributions of apatite grains. (D) Geological cross-section of the central Bitlis Massif (redrawn from Yazgan et al., 1983). See Figure 2 for location of trace of section.

thermal signature of the sediment source rocks contributing detritus to the Muş-Hınıs Basin. In such cases, central ages are hardly significant and only the statistical modeling of FT length distributions can constrain the *T-t* path. Inverse modeling (Fig. 4F) depicts clearly a phase of post-depositional heating (ca. 28–16 Ma; Late Oligocene–Early Miocene), likely resulting from progressive sedimentary burial, followed by mid-Miocene rapid cooling/exhumation starting at ca. 15 Ma.

Sample TU-155 (Eocene sandstone from the Hakkäri Complex mélange; Fig. 2) shows a fairly tight single-grain age distribution and a leptokurtic and unimodal track-length distribution (Figs. 5A, 5C). This translates in a simple thermochronometric evolution (Fig. 5B). The best-fit curve (Fig. 5B) shows (*i*) a phase of progressive heating ranging from deposition to ca. 29 Ma (latest Early Oligocene), followed by a phase of rather stable temperatures (29–13 Ma), in turn followed by rapid uplift starting in the mid-Miocene at ca. 12 Ma.

In summary, modeled samples come from a variety of rock types and tectonostratigraphic units, ranging from (*i*) polymetamorphosed Precambrian basement and (*ii*) its Paleozoic metasedimentary cover, to (*iii*) Eocene sediments incorporated in the frontal part of the Bitlis orogenic wedge and

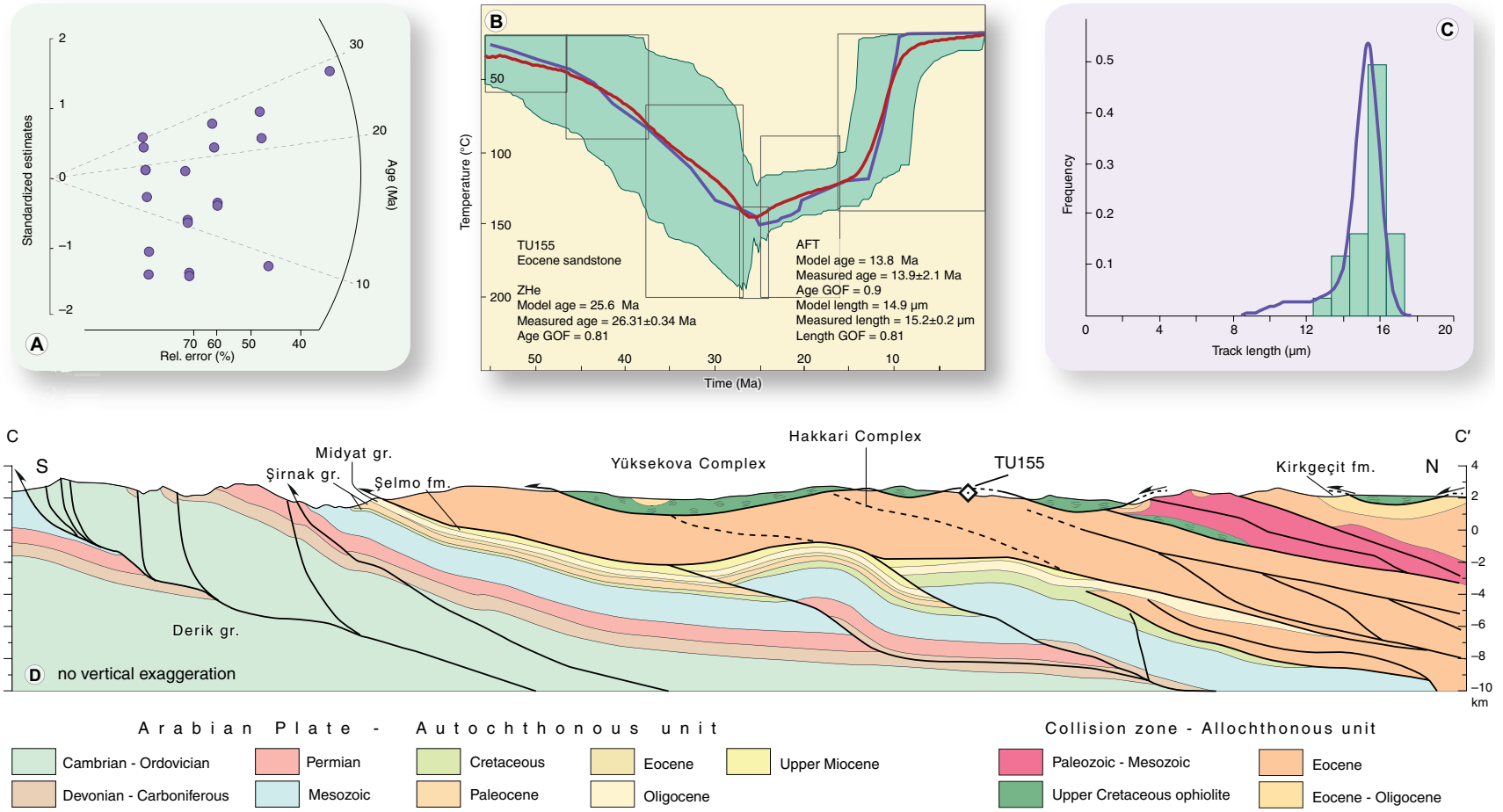

Figure 5. Summary of analytical results for sample TU-155 (Eocene sandstone). See Figure 2 for location. (A) Radial plots of single-grain apatite fission-track (AFT) ages. (B) Time-temperature paths obtained from integrated inverse modeling of AFT data (this study) and (U-Th)/He analyses on zircons (this study). Green areas mark envelopes of statistically acceptable fit, and the thicker lines correspond to the most probable thermal histories: red line is the mean of all statistically acceptable paths; blue line is the best-fit *T-t* path. Parameters related to inverse modeling are reported: GOF, goodness-of-fit gives an indication about the fit between observed and predicted data (values closer to 1 are best). (C) Histogram showing the confined-track length distributions of apatite grains. (D) Geological cross-section of the eastern Bitlis Massif (redrawn from Perinçek, 1990).

(*iv*) Early Oligocene foreland deposits from the Muş-Hınıs Basin north of the Bitlis-Pütürge Massif. Despite such heterogeneity, all analyzed samples point to a coherent thermochronometric history. Most remarkably, they show rather flat *T-t* paths during the Oligocene in the orogenic wedge and a sudden increase in the cooling/exhumation rate in the mid-Miocene, both in the orogenic wedge and the adjacent foreland.

DISCUSSION

The areal distribution of radiometric ages (Fig. 6) in the Bitlis collision zone and its European foreland provides important clues as to the strain distribution pattern through time. Lower temperature radiometric systems (AFT and ZHe) yielded younger ages along a narrow belt coincident with the Bitlis-Pütürge

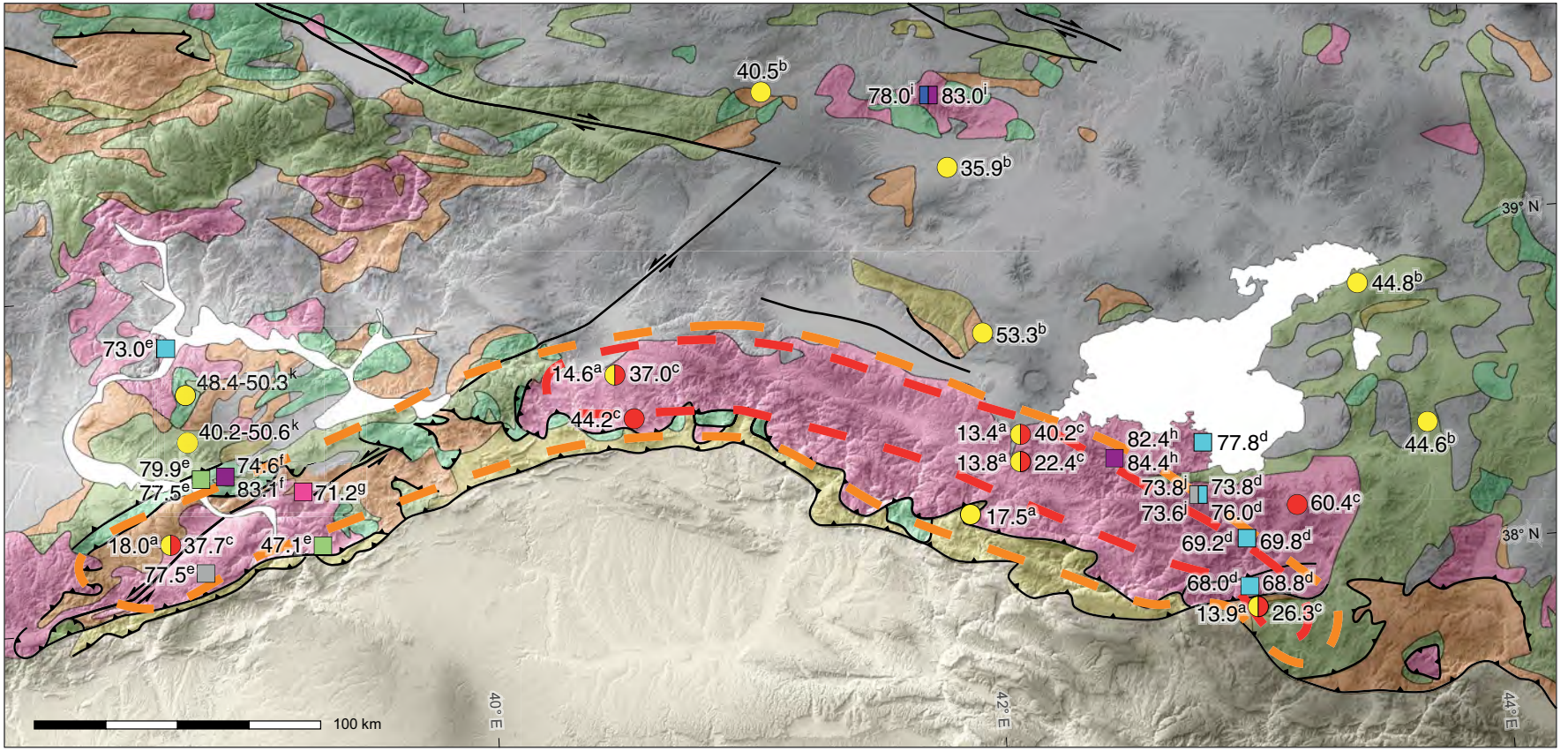

Figure 6. Areal distribution of radiometric ages along the Bitlis-Pütürge collision zone and the Anatolian foreland in southeastern Turkey. Apatite fission-track (AFT) ages are from Table 1; ZrHe ages are from Table 2; all other radiometric ages are from Table 3. Dashed orange line includes all AFT ages younger than 20 Ma; dashed red line includes all AFT ages younger than 15 Ma. Sources of data: [a]Okay et al., 2010; [b]Albino et al., 2013; [c]this paper; [d]Oberhänsli et al., 2012; [e]Rolland et al., 2012; [f]Karaoğlan et al., 2013; [g]Hempton, 1985; [h]Oberhänsli et al., 2013; [i]Topuz et al., 2017; [j]Oberhänsli et al., 2010; [k]Karaoğlan et al., 2016.

collision zone. In the central portion of the belt, AFT central ages cluster tightly between 13.4 ± 2.2 and 14.6 ± 2.5 Ma, i.e., in the mid-Miocene. This cluster resulted from the rapid passage of the samples across the apatite partial annealing zone (~120–60 °C) and registered the last significant cooling/exhumation event suffered by the analyzed rock units. Integrated statistical modeling of all available thermochronological constraints (Ar/Ar, Rb/Sr, U/Pb, ZHe, AFT, stratigraphic relationships) confirm the importance of this sharp and discrete mid-Miocene cooling episode (Figs. 3–5).

AFT central ages from samples taken north of the Bitlis collision zone range consistently between 48.8 and 35.9 Ma (Middle-Late Eocene), not only in the study area but across a wide area comprising most of the eastern Anatolian plateau (Albino et al., 2014), and were not affected by later cooling/exhumation. Middle-Late Eocene cooling is coeval with final closure of the northern Neotethyan branch and the development of the Izmir-Ankara-Erzincan suture zone (Okay and Tüysüz, 1999; Stampfli and Hochard, 2009). In southern Anatolia there is evidence of Eocene extensional tectonics, including the opening of a backarc basin and deposition of a thick volcanosedimentary succession, the Maden Complex (e.g., Yiğitbaş and Yılmaz, 1996; Robertson et al., 2006; Karaoğlan et al., 2016). The relative chronology of these two contrasting tectonic regimes during the Eocene (shortening in central eastern Anatolia and extension in southern eastern Anatolia) has not yet been resolved and requires much additional work.

Results yielded by radiometric systems characterized by a higher closure temperature are age coherent and do not show any areal variation (Fig. 6). In fact, metamorphic rocks of the Bitlis-Pütürge Massif, as well as the other scattered outcrops of metamorphic rocks farther to the north all yielded Late Cretaceous (Campanian-Maastrichtian) metamorphic ages (Hempton, 1985; Oberhänsli et al., 2010, 2012, 2013; Karaoğlan et al., 2013; Rolland et al., 2012). Recent radiometric data by Topuz et al. (2017) indicate that the entire width of the eastern Anatolian Plateau, from the Erzincan-Sevan-Akera suture zone to the north to the Bitlis suture zone to the south, bears the marks of such Late Cretaceous metamorphic event. This implies that the cause of such metamorphism is not to be searched along the Bitlis collision zone.

The stratigraphy of the northernmost sector of the Arabian platform provides a compelling record of the tectonic evolution of the adjacent Bitlis-Pütürge orogenic prism as it has been the lower plate of the Arabia-Eurasia subduction/collision zone during the entire Cenozoic. Two coarse-grained clastic inputs punctuate the stratigraphy of the northern Arabian platform south of the collision zone. The first one occurred in the Late Cretaceous (Late Campanian-Maastrichtian: Antak Formation, Tanjero Formation, and equivalents) and was related to the creation of structural relief, lithospheric flexure, and creation of accommodation resulting from widespread ophiolite obduction over the Arabian platform and related crustal shortening. Such a discrete and important episode of ophiolite obduction along the Anatolide-Tauride and Arabian northern continental margins has been described from western Anatolia to Oman (e.g., Coleman, 1981; Okay et al., 2001; Robertson, 2002) and is discussed further below. The second influx of coarse-grained clastics occurred in the Late Miocene (Şelmo Formation and its lateral equivalents) and is commonly interpreted as marking the onset of hard collision. These two clastic intervals are separated by Paleogene carbonate sediments and no coherent collision-related foreland basin stratigraphy for the Oligocene can be outlined (Fig. 7). If the Arabia-Eurasia collision took place in the Oligocene one would expect the presence of large volumes of orogen-derived sediments on the flexured lower (Arabian) plate, whereas the Oligocene succession south of the Bitlis-Pütürge orogenic prism lacks any evidence of synorogenic sedimentation (see also Robertson et al., 2016). The Oligocene stratigraphic hiatus (considered by some as evidence of collision-related tectonic deformation) may well be explained by the Oligocene eustatic sea level lowstand, one of the largest in Earth's history. Miller et al. (2008) concluded that a glacioeustatic sea level lowering of 55 m occurred in the Early Oligocene (35.7–33.5 Ma). Such sea level fall produced dramatic paleoenvironmental and stratigraphic changes in the Arabian flatlands (Nairn and Alsharhan, 1997; Jassim and Goff, 2006) and can account for the widespread Oligocene nondepositional hiatus. Therefore, we conclude that there is no stratigraphic evidence on the Arabian margin for an Oligocene collision with the Anatolide-Tauride terrane to the north. The thermochronometric reconstructions presented here (Figs. 3–5) underline the absence of significant Oligocene cooling/exhumation along the southern margin of the Anatolide-Tauride terrane and point instead to rapid cooling/exhumation in the Miocene, in agreement with field stratigraphic and structural relationships. A subsidence curve from the portion of the Muş-Hınıs retroarc foreland basin north of Lake Van also show a discrete episode of uplift in the mid-Miocene within the overall context of protracted subsidence typical of upper-plate (retroarc) foreland basins (Fig. 8).

Geological field evidence indicates that a large area south of the Erzincan-Sevan suture was covered by a series of large obducted ophiolites by mid-Campanian time. These took the form of either large, relatively coherent slabs now cropping out as klippen or widespread mélange bodies (Bilgic, 2002; Günay and Şenel, 2002; Şenel and Ercan, 2002; Tarhan, 2002). At the same time, the same area experienced *HP-LT* metamorphism (Hempton, 1985; Okay et al., 1985, Oberhänsli et al., 2010, 2012, 2013; Rolland et al., 2012; Topuz et al., 2017). For example, across the Pütürge Massif the basement complex and the metamorphic sole of the overlying ophiolitic nappes yielded virtually the same Late Cretaceous metamorphic ages [77.5 ± 0.7 Ma (Ar/Ar on phengites) and 78.7 ± 1.0 Ma (Ar/Ar on amphibole), respectively] (Fig. 3D; Table 3). North of the Pütürge Massif, other scattered inliers of metasedimentary rocks interspersed within the widespread volcano-sedimentary cover of the Anatolian Plateau yielded consistent Late Cretaceous metamorphic ages (Topuz et al., 2017). The radiometric data set is far from being complete, but the picture emerging in eastern Anatolia is one of a coherent metamorphic event across the entire area located between the Erzincan-Sevan suture to the north and the Assyrian suture to the south. This metamorphism is coeval with massive southward ophiolite obduction from the northern branch of the Neotethys onto the Anatolide-Tauride terrane (Stampfli and Hochard, 2009) (Fig. 9A).

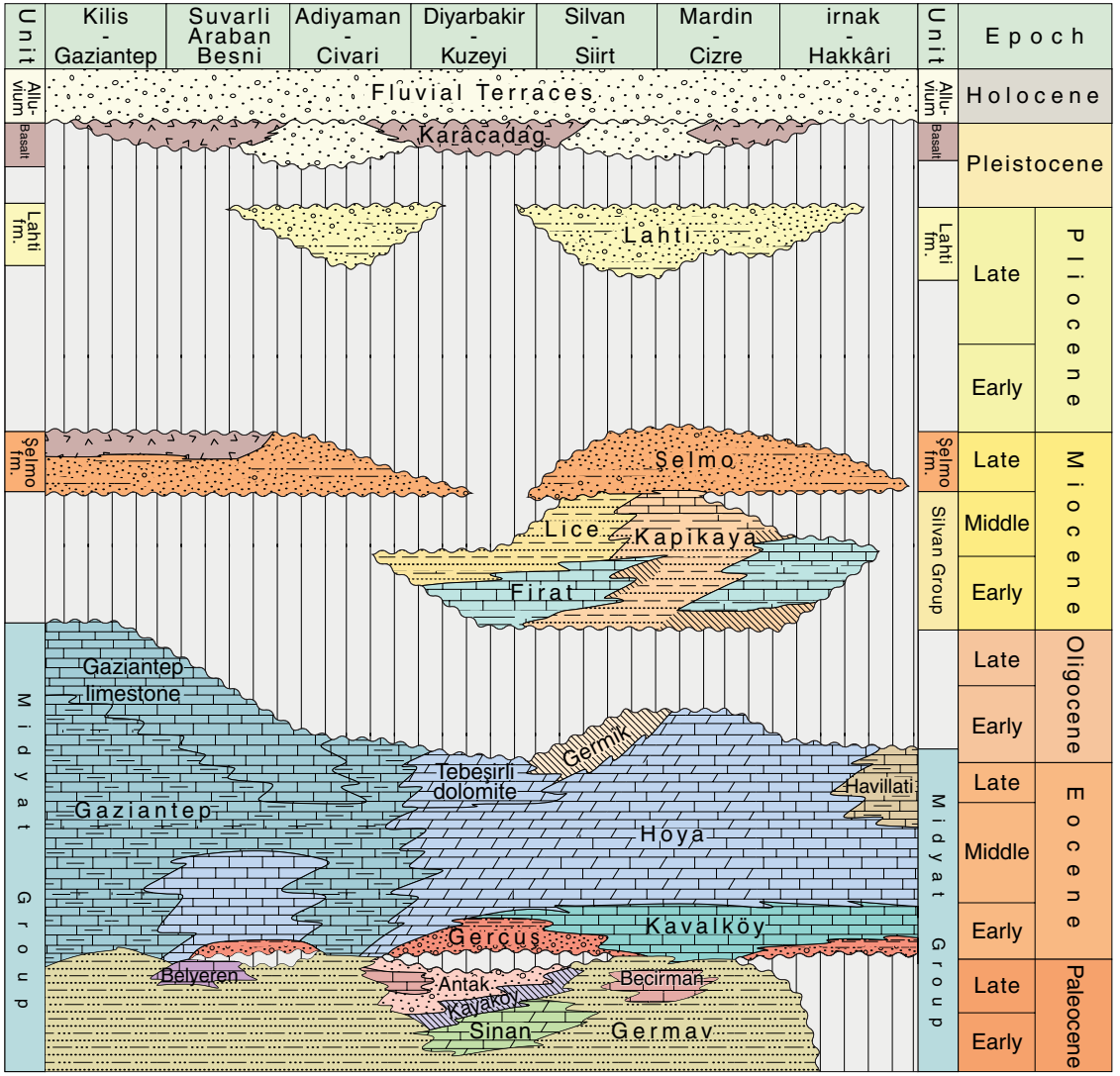

Figure 7. Chronolithostratigraphic chart for the northernmost Arabian platform in Turkish territory (from Yılmaz and Duran, 1997).

In the past, the pre-Neogene basement of the Eastern Anatolia plateau has been interpreted as consisting largely of an accretionary prism spanning (north to south) the distance from the eastern Pontides to the Bitlis collision zone (Eastern Anatolia accretionary complex [EAAC]; Şengör and Yılmaz, 1981; Şengör et al., 2003). The EAAC concept has had wide resonance and is now ingrained in the scientific literature. However, recent field and laboratory data indicate that eastern Anatolia is instead characterized by continental assemblages that underwent high-temperature and medium-pressure metamorphism at middle- to lower-crustal depths during the Late Cretaceous (Yılmaz et al., 2010; Topuz et al., 2017), as discussed above. These continental assemblages are tectonically overlain by disrupted ophiolites or ophiolitic mélange obducted in the Late Cretaceous and then pushed southward during

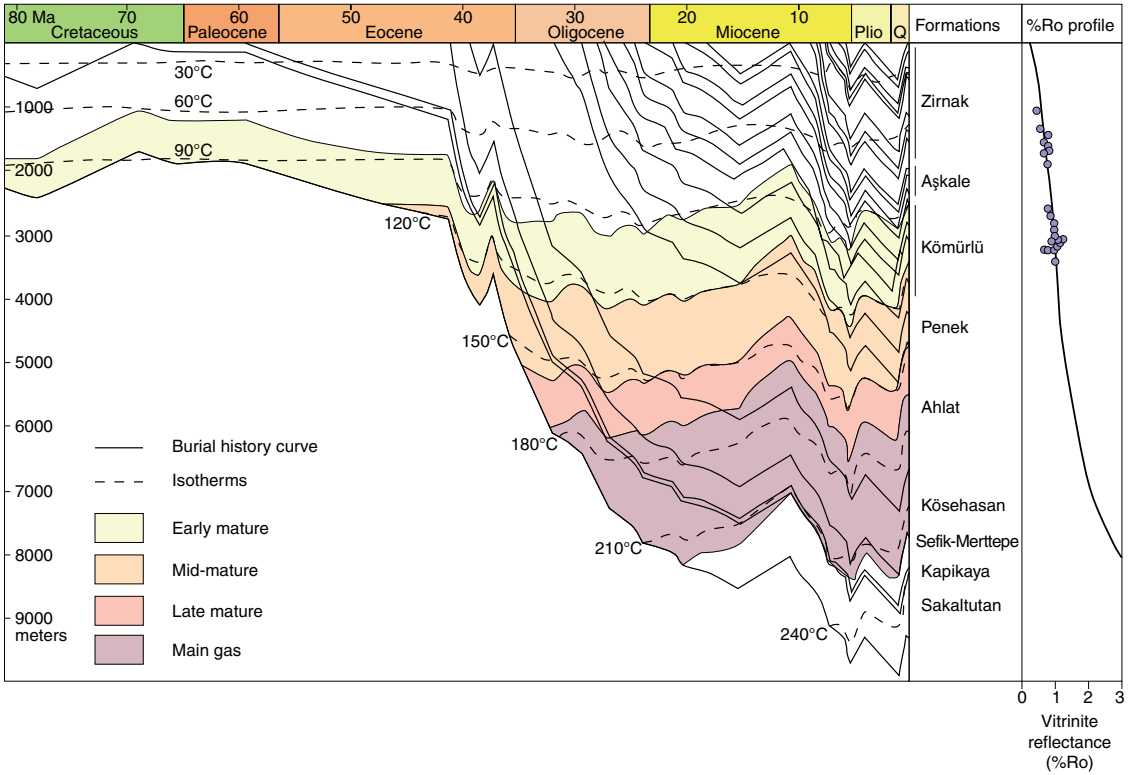

Figure 8. Burial and subsidence history, isotherms, and vitrinite reflectance (%Ro) profile for the Malazgirt-1 well (for location, see Fig. 2) in the eastern Muş-Hınıs Basin (redrawn from Huvaz, 2009). Inception of subsidence at the Middle-Late Eocene transition coincides with the beginning of subduction along the southern margin of the Anatolide-Tauride block. Subsidence continued until the mid-Miocene in a foreland basin setting, when a discrete phase of inversion occurred.

the closure of the northern branch of the Neotethys and the ensuing development of the Izmir-Ankara-Erzincan suture zone (e.g., Okay and Tüysüz, 1999). The synchronicity of obduction and widespread metamorphism as well as the structural relationship between the ophiolites and the underlying continental basement support the hypothesis that the emplacement of a large ophiolitic nappe complex was responsible for diffuse deformation and metamorphism of the underlying Paleozoic sedimentary cover of the Proterozoic basement complex of the Anatolide-Tauride terrane. According to Topuz et al. (2017), there is no indication of major strike-slip faults which might have interposed the continental fragments within the ophiolites and hence the scattered metamorphic inliers are interpreted to be the evidence of a more or less continuous continental substrate overthrust by the ophiolitic nappe complex. Ophiolite obduction took place in the Campanian (Fig. 9A), but southward tectonic transport of ophiolitic nappes (possibly including also sections of the underlying metamorphosed Paleozoic sedimentary cover of the Anatolide-Tauride terrane) continued during the Maastrichtian and the Paleocene (Fig. 9B) as the collision between the Anatolide-Tauride and Sakarya terranes was progressing. By the Middle Eocene (Fig. 9C) collision along the Izmir-Ankara-Erzincan suture zone was complete and subduction jumped to the southern margin of the Anatolide-Tauride terrane. The convergence rate between Africa and the southern margin of Eurasia (actually a collage of Gondwana-derived exotic terranes) had decreased, the subducting slab was affected by roll-back, and the upper plate underwent extension. Such extension is recorded by the Maden Complex, a mid-Eocene volcano-sedimentary succession developed in a back-arc basin (Yiğitbaş and Yılmaz, 1996) and presently occurring as intensely deformed tectonostratigraphic units within the Bitlis-Pütürge orogenic wedge. Widespread extension along the southern margin of the Anatolide-Tauride terrane as recorded by the Maden basin(s) is hardly compatible with the notion of an Eocene Arabia-Eurasia collision.

Low-temperature thermochronological data for the Eurasian foreland north of the Bitlis- Pütürge suture zone suggest that the tectonic stresses related to the Arabian collision were transmitted efficiently over large distances, focusing preferentially at rheological discontinuities located as far as the Eastern Pontides and the Lesser Caucasus (Albino et al., 2014; Cavazza et al., 2017). Stress focused either (*i*) along the marked rheological difference between the

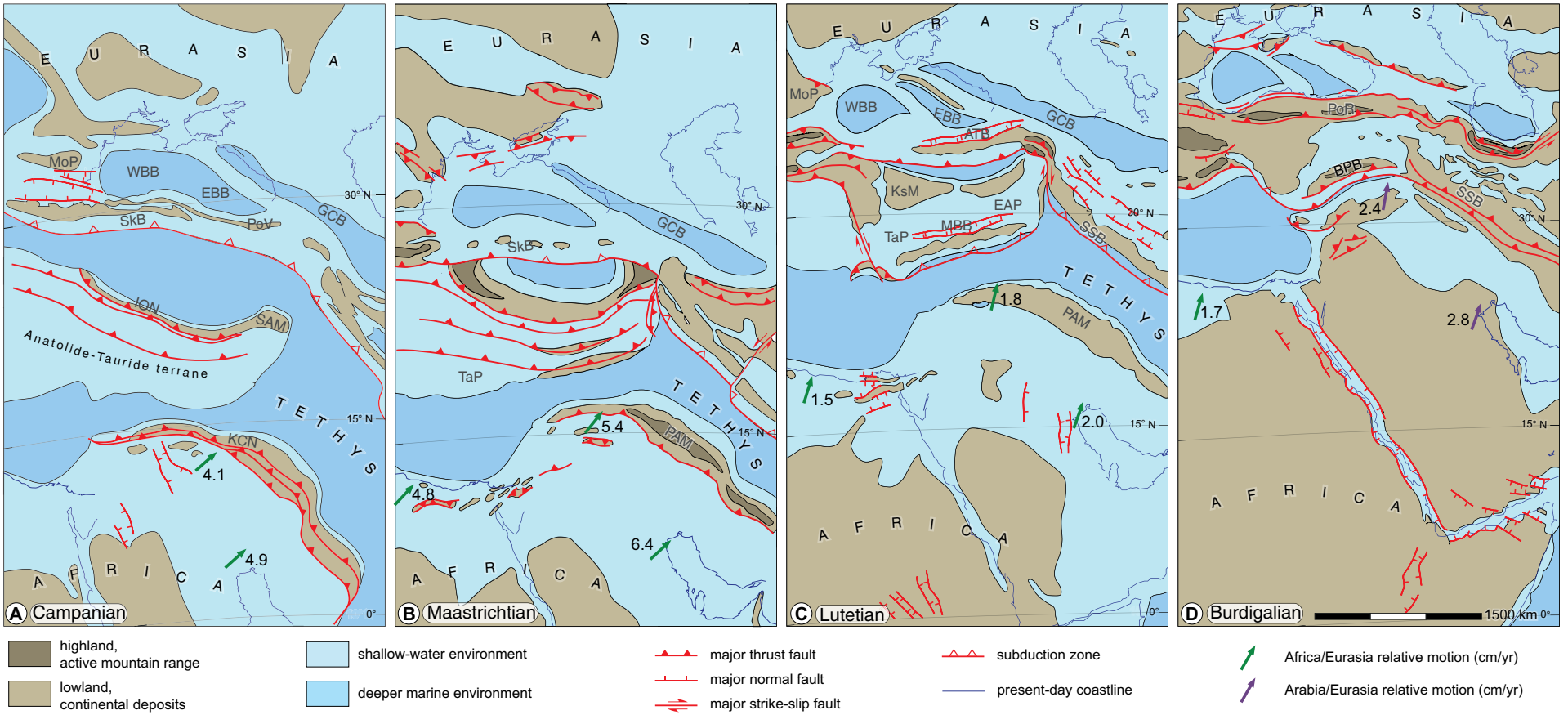

Figure 9. Paleogeographic sketch maps for the Arabia-Eurasia collision (modified from Barrier and Vrielynk, 2008). ATB—Anatolia-Tauride block; EAP—eastern Anatolia platform; EBB—eastern Black Sea basin; GCB—Greater Caucasus Basin; ION—Izmir-Ankara-Erzincan ophiolite nappes; KCN—Kizildag-Cilo ophiolite nappe; KsM—Kirsehir Massif; MBB—Maden backarc basin; MoP—Moesian Platform; PAM—peri-Arabian massif; PoR—Pontides Range; PoV—Pontide volcanic arc; SAM—Sevan-Akera ophiolitic massif; SkB—Sakarya Basin; SSB—Sanandaj-Sirjan block; TaP—Tauride platform; WBB—western Black Sea basin.

polydeformed continental lithosphere of the Eastern Pontides and the relatively pristine quasi-oceanic lithosphere of the eastern Black Sea or (*ii*) along properly oriented segments of the Erzincan-Sevan-Akera suture zone. Since the late Middle Miocene, a new tectonic regime has been active. The westward translation of Anatolia currently accommodates most of the Arabia-Eurasia convergence, thus decoupling the foreland from the orogenic wedge and precluding efficient northward stress transfer. As soon as the two plates were mechanically coupled, the inception of the Northern and Eastern Anatolian fault systems absorbed much of the plate convergence. Tectonic escape of Anatolia was preconditioned and facilitated by slab rollback along the Aegean subduction zone (Jolivet and Brun, 2010).

CONCLUSIONS

Noble gas and fission-track thermochronometric data—integrated with radiometric data from the literature and the analysis of field stratigraphic and structural relationships—constrain the overall thermal history of the Bitlis-Pütürge metamorphic complex, i.e., the area of maximum indentation along the Assyrian-Zagros continental collision zone. The data set indicates widespread latest Cretaceous metamorphism of a passive margin sedimentary sequence and its igneous basement along the suture zone and across the entire width of the Anatolia-Tauride block north of the suture. This metamorphism is likely related to extensive southward obduction of oceanic lithosphere from the

northern branch of the Neotethys onto the northern continental margin of the Anatolide-Tauride block. Evidence for this interpretation lies in the occurrence of Late Cretaceous metamorphic rocks extending from the Izmir-Ankara-Erzincan suture to the north to the Bitlis-Pütürge metamorphic complex to the south. The basement complex of the Bitlis and Pütürge massifs along the suture was then rapidly exhumed between ca. 65 and 55 Ma and eventually overlain by Eocene shallow marine sediments. Integrated statistical modeling shows that the Oligocene thermochronometric evolution of the orogen was rather featureless, contrary to the widely held belief that this epoch marked the beginning of the Arabia-Eurasia collision and was thus characterized by widespread deformation. Conversely, during the Middle Miocene, the Bitlis-Pütürge orogenic wedge was rapidly and significantly deformed both by (*i*) frontal accretion, as shown by cooling/exhumation of the foreland deposits on both sides of the orogenic prism, and (*ii*) underplating, as shown by cooling/exhumation of the central metamorphic core of the orogenic wedge. Orogenic growth is also substantiated by the stratigraphy of the lower (Arabian) plate, which shows the presence of a coarse-grained clastic wedge in the Middle Miocene as well as evidence of growth structures.

Taking into consideration that colliding continental margins are morphologically irregular and strain sequences are commonly diachronous along the strike of suture zones (Dewey et al., 1986), we emphasize that the results of this study applies only to the Bitlis-Pütürge sector of the Arabia-Eurasia collision zone and should not be necessarily applied also to the Zagros collision front to the southeast.

ACKNOWLEDGMENTS

Thanks to Olivier Lacombe, Federico Rossetti and Gerard Stampfli for fruitful discussions, and to Uttam Chowdhury for analytical assistance with the zircon He dating. The authors would like to thank the anonymous reviewers and Associate Editor Mike Williams for their valuable comments and suggestions to improve the quality of the paper. This research was funded by MIUR (Italian Ministry of Education, University and Research) and the University of Bologna (RFO funds).

REFERENCES CITED

Agard, P., Omrani, J., Jolivet, L., and Mouthereau, F., 2005, Convergence history across Zagros (Iran): Constraints from collisional and earlier deformation: International Journal of Earth Sciences, v. 94, p. 401–419, https://doi.org/10.1007/s00531-005-0481-4.

Akay, E., Erkan, E., and Ünay, E., 1989, Stratigraphy of the Tertiary Muş basin [in Turkish]: Bulletin of the Mineral Research and Exploration Institute (MTA) of Turkey, v. 109, p. 59–76.

Alavi, M., 1994, Tectonics of the Zagros orogenic belt of Iran: New data and interpretations: Tectonophysics, v. 229, p. 211–238, https://doi.org/10.1016/0040-1951(94)90030-2.

Albino, I., Cavazza, W., Zattin, M., Okay, A.I., Adamia, S., and Sadradze, N., 2014, Far-field tectonic effects of the Arabia-Eurasia collision and the inception of the North Anatolian Fault system: Geological Magazine, v. 151, p. 372–379, https://doi.org/10.1017/S0016756813000952.

Allen, M.B., and Armstrong, H.A., 2008, Arabia–Eurasia collision and the forcing of mid-Cenozoic global cooling: Palaeogeography, Palaeoclimatology, Palaeoecology, v. 265, p. 52–58, https://doi.org/10.1016/j.palaeo.2008.04.021.

Barazangi, M., Sandvol, E., and Seber, D., 2006, Structure and tectonic evolution of the Anatolian plateau in eastern Turkey, *in* Dilek, Y., and Pavlides, S., eds., Postcollisional Tectonics and Magmatism in the Mediterranean Region and Asia: Geological Society of America Special Paper, v. 409, p. 463–473, https://doi.org/10.1130/2006.2409(22).

Barrier, E., and Vrielynk, B., 2008, Palaeotectonic Maps of the Middle East–Middle East Basins Evolution (MEBE) Programme: Paris, France, Commission for the Geological Map of the World, scale 1:18,500,000.

Berberian, M., and King, G.C.P., 1981, Towards a paleogeography and tectonic evolution of Iran: Canadian Journal of Earth Sciences, v. 18, p. 210–265, https://doi.org/10.1139/e81-019.

Beyarslan, M., Lın, Y.C., Bingöl, A.F., and Chung, S.L., 2016, Zircon U-Pb age and geochemical constraints on the origin and tectonic implication of Cadomian (Ediacaran-Early Cambrian) magmatism in SE Turkey: Journal of Asian Earth Sciences, v. 130, p. 223–238, https://doi.org/10.1016/j.jseaes.2016.08.006.

Bilgic, T., 2002, Turkey Geological Map, Sheet Sivas: Ankara, Turkey, Maden Tetkik ve Arama Genel Müdürlüğü, scale 1:500,000.

Cavazza, W., Albino, I., Zattin, M., Galoyan, G., Imamverdiyev, N., and Melkonyan, R., 2017, Thermochronometric evidence for Miocene tectonic reactivation of the Sevan–Akera suture zone (Lesser Caucasus): A far-field tectonic effect of the Arabia–Eurasia collision?, *in* Sosson, M., et al., eds., Tectonic Evolution of the Eastern Black Sea and Caucasus: Geological Society of London, Special Publications, v. 428, p. 187–198, https://doi.org/10.1144/SP428.4.

Coleman, R.G., 1981, Tectonic setting for ophiolite obduction in Oman: Journal of Geophysical Research. Solid Earth, v. 86, p. 2497–2508, https://doi.org/10.1029/JB086iB04p02497.

Dewey, J.F., Hempton, M.R., Kidd, W.S.F., Saroglu, F., and Şengör, A.M.C., 1986, Shortening of continental lithosphere: The neotectonics of Eastern Anatolia—a young collision zone, *in* Coward, M.P., and Ries, A.C., eds., Collision Tectonics: Geological Society of London Special Publication 19, p. 1–36, https://doi.org/10.1144/GSL.SP.1986.019.01.01.

Donelick, R.A., O'Sullivan, P.B., and Ketcham, R.A., 2005, Apatite fission-track analysis: Reviews in Mineralogy and Geochemistry, v. 58, p. 49–94, https://doi.org/10.2138/rmg.2005.58.3.

Ehlers, T.A., Chaudhri, T., Kumar, S., Fuller, C.W., Willett, S.D., Ketcham, R.A., Brandon, M.T., Belton, D.X., Kohn, B.P., Gleadow, A.J., and Dunai, T.J., 2005, Computational tools for low-temperature thermochronometer interpretation: Reviews in Mineralogy and Geochemistry, v. 58, p. 589–622, https://doi.org/10.2138/rmg.2005.58.22.

Göncüoğlu, M.C., and Turhan, N., 1984, Geology of the Bitlis metamorphic belt, *in* Tekeli, O., and Göncüoğlu, M.C., eds., Proceedings of the International Symposium on the Geology of the Taurus Belt, Ankara, Turkey, p. 237–244.

Günay, Y., and Şenel, M., 2002, Turkey Geological Map, Sheet Cizre: Ankara, Turkey: Maden Tetkik ve Arama Genel Müdürlüğü, scale 1:500,000.

Hall, R., 1976, Ophiolite emplacement and the evolution of the Taurus suture zone, southeastern Turkey: Geological Society of America Bulletin, v. 87, no. 7, p. 1078–1088, https://doi.org/10.1130/0016-7606(1976)87<1078:OEATEO>2.0.CO;2.

Hempton, M.R., 1985, Structure and deformation history of the Bitlis suture near Lake Hazar, southeastern Turkey: Geological Society of America Bulletin, v. 96, p. 233–243, https://doi.org/10.1130/0016-7606(1985)96<233:SADHOT>2.0.CO;2.

Hourigan, J.K., Reiners, P.W., and Brandon, M.T., 2005, U-Th zonation-dependent alpha-ejection in (U-Th)/He chronometry: Geochimica et Cosmochimica Acta, v. 69, p. 3349–3365, https://doi.org/10.1016/j.gca.2005.01.024.

Hurford, A.J., and Green, P.F., 1983, The zeta age calibration of fission-track dating: Chemical Geology, v. 41, p. 285–317, https://doi.org/10.1016/S0009-2541(83)80026-6.

Hüsing, S.K., Zachariasse, W.J., Van Hinsbergen, D.J., Krijgsman, W., Inceöz, M., Harzhauser, M., Mandic, O., and Kroh, A., 2009, Oligocene–Miocene basin evolution in SE Anatolia, Turkey: Constraints on the closure of the eastern Tethys gateway, *in* Van Hinsbergen, D.J.J., et al., eds., Collision and Collapse at the Africa-Arabia-Eurasia Subduction Zone: Geological Society of London Special Publication 311, p. 107–132, https://doi.org/10.1144/SP311.4.

Huvaz, O., 2009, Comparative petroleum systems analysis of the interior basins of Turkey: Implications for petroleum potential: Marine and Petroleum Geology, v. 26, p. 1656–1676, https://doi.org/10.1016/j.marpetgeo.2009.05.002.

Jassim, S.Z., and Goff, J.C., eds., 2006, Geology of Iraq: Prague, Czech Republic, DOLIN sro, 341 p., http://www.dolin-sro.cz/geology.html (distributed by Geological Society of London).

Jolivet, L., and Brun, J.P., 2010, Cenozoic geodynamic evolution of the Aegean: International Journal of Earth Sciences, v. 99, p. 109–138, https://doi.org/10.1007/s00531-008-0366-4.

Jolivet, L., and Faccenna, C., 2000, Mediterranean extension and the Africa-Eurasia collision: Tectonics, v. 19, no. 6, p. 1095–1106, https://doi.org/10.1029/2000TC900018.

Karaoğlan, F., Parlak, O., Robertson, A., Thöni, M., Klötzli, U., Koller, F., and Okay, A.I., 2013, Evidence of Eocene high-temperature/high-pressure metamorphism of ophiolitic rocks and granitoid intrusion related to Neotethyan subduction processes (Doğanşehir area, SE

Anatolia), *in* Robertson, A.H.F., et al., eds., Geological Development of Anatolia and the Easternmost Mediterranean Region: Geological Society of London Special Publication 372, p. 249–272, https://doi.org/10.1144/SP372.21.

Karaoğlan, F., Parlak, O., Hejl, E., Neubauer, F., and Kloetzli, U., 2016, The temporal evolution of the active margin along the Southeast Anatolian Orogenic Belt (SE Turkey): Evidence from U–Pb, Ar–Ar and fission track chronology: Gondwana Research, v. 33, p. 190–208, https://doi.org/10.1016/j.gr.2015.12.011.

Ketcham, R.A., 2005, Forward and inverse modeling of low-temperature thermochronometry data: Reviews in Mineralogy and Geochemistry, v. 58, no. 1, p. 275–314, https://doi.org/10.2138/rmg.2005.58.11.

Ketcham, R.A., Carter, A., Donelick, R.A., Barbarand, J., and Hurford, A.J., 2007, Improved modeling of fission-track annealing in apatite: American Mineralogist, v. 92, no. 5–6, p. 799–810, https://doi.org/10.2138/am.2007.2281.

Kiliç, A.D., and Ateş, C., 2015, Geochronology of the Late Cretaceous magmatism and metamorphism, Pütürge massif, Turkey: Yanshi Xuebao, v. 31, p. 1485–1493.

Le Pichon, X., and Kreemer, C., 2010, The Miocene-to-present kinematic evolution of the eastern Mediterranean and Middle East and its implications for dynamics: Annual Review of Earth and Planetary Sciences, v. 38, p. 323–351, https://doi.org/10.1146/annurev-earth-040809-152419.

McQuarrie, N., and van Hinsbergen, D.J., 2013, Retrodeforming the Arabia-Eurasia collision zone: Age of collision versus magnitude of continental subduction: Geology, v. 41, p. 315–318, https://doi.org/10.1130/G33591.1.

Miller, K.G., Browning, J.V., Aubry, M.P., Wade, B.S., Katz, M.E., Kulpecz, A.A., and Wright, J.D., 2008, Eocene–Oligocene global climate and sea-level changes: St. Stephens Quarry, Alabama: Geological Society of America Bulletin, v. 120, p. 34–53, https://doi.org/10.1130/B26105.1.

Nairn, A.E.M., and Alsharhan, A.S., 1997, Sedimentary Basins and Petroleum Geology of the Middle East: Amsterdam, Netherlands, Elsevier, 878 p.

Oberhänsli, R., Candan, O., Bousquet, R., Rimmele, G., Okay, A.I., and Goff, J., 2010, Alpine high pressure evolution of the eastern Bitlis complex, SE Turkey, *in* Sosson, M., et al., eds., Sedimentary Basin Tectonics from the Black Sea and Caucasus to the Arabian Platform: Geological Society of London Special Publication 340, p. 461–483, https://doi.org/10.1144/SP340.20.

Oberhänsli, R., Bousquet, R., Candan, O., and Okay, A.I., 2012, Dating subduction events in East Anatolia, Turkey: Turkish Journal of Earth Sciences, v. 21, p. 1–17.

Oberhänsli, R., Koralay, E., Candan, O., Pourteau, A., and Bousquet, R., 2013, Late Cretaceous eclogitic high-pressure relics in the Bitlis Massif: Geodinamica Acta, v. 26, p. 175–190, https://doi.org/10.1080/09853111.2013.858951.

Okay, A.I., 2008, Geology of Turkey: A synopsis: Anschnitt, v. 21, p. 19–42.

Okay, A.I., and Tüysüz, O., 1999, Tethyan sutures of northern Turkey, *in* Durand, B., et al., eds., The Mediterranean Basins: Tertiary Extension within the Alpine Orogen: Geological Society of London Special Publication 156, p. 475–515, https://doi.org/10.1144/GSL.SP.1999.156.01.22.

Okay, A.I., Arman, M.B., and Göncüoğlu, M.C., 1985, Petrology and phase relations of the kyanite-eclogites from eastern Turkey: Contributions to Mineralogy and Petrology, v. 91, p. 196–204, https://doi.org/10.1007/BF00377767.

Okay, A.I., Tansel, İ., and Tüysüz, O., 2001, Obduction, subduction and collision as reflected in the Upper Cretaceous–Lower Eocene sedimentary record of western Turkey: Geological Magazine, v. 138, p. 117–142, https://doi.org/10.1017/S0016756801005088.

Okay, A.I., Zattin, M., and Cavazza, W., 2010, Apatite fission-track data for the Miocene Arabia-Eurasia collision: Geology, v. 38, p. 35–38, https://doi.org/10.1130/G30234.1.

Perinçek, D., 1990, Stratigraphy of the Hakkäri province, southeast Turkey [in Turkish]: TAPG Bulletin, v. 2, no. 1, p. 21–68.

Reiners, P.W., 2005, Zircon (U-Th)/He thermochronometry: Reviews in Mineralogy and Geochemistry, v. 58, p. 151–179, https://doi.org/10.2138/rmg.2005.58.6.

Reiners, P.W., and Brandon, M.T., 2006, Using thermochronology to understand orogenic erosion: Annual Review of Earth and Planetary Sciences, v. 34, p. 419–466, https://doi.org/10.1146/annurev.earth.34.031405.125202.

Robertson, A.H.F., 2002, Overview of the genesis and emplacement of Mesozoic ophiolites in the Eastern Mediterranean Tethyan region: Lithos, v. 65, p. 1–67, https://doi.org/10.1016/S0024-4937(02)00160-3.

Robertson, A.H., Ustaömer, T., Parlak, O., Ünlügenç, U.C., Taşlı, K., and Inan, N., 2006, The Berit transect of the Tauride thrust belt, S Turkey: Late Cretaceous–Early Cenozoic accretionary/collisional processes related to closure of the Southern Neotethys: Journal of Asian Earth Sciences, v. 27, p. 108–145, https://doi.org/10.1016/j.jseaes.2005.02.004.

Robertson, A.H.F., Parlak, O., Rizaoğlu, T., Ünlügenç, Ü., İnan, N., Tasli, K., and Ustaömer, T., 2007, Tectonic evolution of the South Tethyan ocean: Evidence from the Eastern Taurus Mountains (Elazığ region, SE Turkey), *in* Ries, A.C., ed., Deformation of the Continental Crust: The Legacy of Mike Coward: Geological Society of London Special Publication 272, p. 231–270, https://doi.org/10.1144/GSL.SP.2007.272.01.14.

Robertson, A., Boulton, S.J., Taslı, K., Yıldırım, N., İnan, N., Yıldız, A., and Parlak, O., 2016, Late Cretaceous–Miocene sedimentary development of the Arabian continental margin in SE Turkey (Adıyaman region): Implications for regional palaeogeography and the closure history of southern Neotethys: Journal of Asian Earth Sciences, v. 115, p. 571–616, https://doi.org/10.1016/j.jseaes.2015.01.025.

Rolland, Y., Perinçek, D., Kaymakci, N., Sosson, M., Barrier, E., and Avagyan, A., 2012, Evidence for ~80–75 Ma subduction jump during Anatolide–Tauride–Armenian block accretion and ~48 Ma Arabia–Eurasia collision in Lesser Caucasus–East Anatolia: Journal of Geodynamics, v. 56, p. 76–85, https://doi.org/10.1016/j.jog.2011.08.006.

Sancay, R.H., Bati, Z., and Işik, U., 2006, Palynomorph, foraminifera, and calcareous nannoplankton biostratigraphy of Oligo–Miocene sediments in the Muş Basin, Eastern Anatolia, Turkey: Turkish Journal of Earth Sciences, v. 15, p. 259–319.

Şenel, M., and Ercan, T., 2002, Turkey Geological Map, Sheet Van: Ankara, Turkey, Maden Tetkik ve Arama Genel Müdürlüğü, scale 1:500,000.

Şengör, A.M.C., and Kidd, W.S.F., 1979, Post-collisional tectonics of the Turkish-Iranian plateau and a comparison with Tibet: Tectonophysics, v. 55, p. 361–376, https://doi.org/10.1016/0040-1951(79)90184-7.

Şengör, A.M.C., and Yılmaz, Y., 1981, Tethyan evolution of Turkey: A plate tectonic approach: Tectonophysics, v. 75, p. 181–241, https://doi.org/10.1016/0040-1951(81)90275-4.

Şengör, A.M.C., Görür, N., and Şaroğlu, F., 1985, Strike-slip faulting and related basin formation in zones of tectonic escape: Turkey as a case study, *in* Biddle, K.D., and Christie-Blick, N., eds., Strike-slip deformation, basin formation and sedimentation: Society of Economic Paleontologists and Mineralogists Special Publication 17, p. 227–264.

Şengör, A.M.C., Özeren, S., Genc, T., and Zor, E., 2003, East Anatolian high plateau as a mantle-supported, north-south shortened domal structure: Geophysical Research Letters, v. 30, https://doi.org/10.1029/2003GL017858.

Şengör, A.C., Özeren, M.S., Keskin, M., Sakınç, M., Özbakır, A.D., and Kayan, I., 2008, Eastern Turkish high plateau as a small Turkic-type orogen: Implications for post-collisional crust-forming processes in Turkic-type orogens: Earth-Science Reviews, v. 90, p. 1–48, https://doi.org/10.1016/j.earscirev.2008.05.002.

Stampfli, G.M., and Hochard, C., 2009, Plate tectonics of the Alpine realm, *in* Murphy, J.B., et al., eds., Ancient Orogens and Modern Analogues: Geological Society of London, Special Publications, v. 327, p. 89–111, https://doi.org/10.1144/SP327.6.

Tarhan, N., 2002, Turkey Geological Map, Sheet Erzurum: Maden Tetkik ve Arama Genel Müdürlüğü, Ankara, Turkey, 2nd edition, scale 1:500,000.

Topuz, G., Candan, O., Zack, T., and Yılmaz, A., 2017, East Anatolian plateau constructed over a continental basement: No evidence for the East Anatolian accretionary complex: Geology, v. 45, p. 791–794, https://doi.org/10.1130/G39111.1.

Yazgan, E., Michard, A., Whitechurch, H., and Montigny, R., 1983, Le Taurus de Malatya (Turquie orientale), élément de la suture sud-tèthysienne: Bulletin de la Société Géologique de France, v. 25, p. 59–69, https://doi.org/10.2113/gssgfbull.S7-XXV.1.59.

Yiğitbaş, E., and Yılmaz, Y., 1996, New evidence and solution to the Maden complex controversy of the Southeast Anatolian orogenic belt (Turkey): Geologische Rundschau, v. 85, p. 250–263, https://doi.org/10.1007/BF02422232.

Yılmaz, Y., 1993, New evidence and model on the evolution of the southeast Anatolian orogen: Geological Society of America Bulletin, v. 105, p. 251–271, https://doi.org/10.1130/0016-7606(1993)105<0251:NEAMOT>2.3.CO;2.

Yılmaz, E., and Duran, O., 1997, Stratigraphic lexicon for the autochthonous and allochthonous units of Southeast Anatolia [in Turkish]: Türkiye Petrolleri A.O. Research Center, Publication No. 31, 460 p.

Yılmaz, A., Yılmaz, H., Kaya, C., and Boztug, D., 2010, The nature of the crustal structure of the Eastern Anatolian Plateau, Turkey: Geodinamica Acta, v. 23, p. 167–183, https://doi.org/10.3166/ga.23.167-183.